Copyright Notice

Huckemann, S.; Hotz, T.; Munk, A.: *Global Models for the Orientation Field of Fingerprints: An Approach Based on Quadratic Differentials,* IEEE Transactions on Pattern Analysis and Machine Intelligence, **30**(9), pp. 1507–1519, Sept. 2008.

Digital Object Identifier: `doi://10.1109/TPAMI.2007.70826`

URL: `http://ieeexplore.ieee.org/stamp/stamp.jsp?arnumber=4407717&isnumber=4567786`

Global Models for the Orientation Field of Fingerprints: An Approach Based on Quadratic Differentials

Stephan Huckemann, Thomas Hotz, and Axel Munk

Abstract—Quadratic differentials naturally define analytic orientation fields on planar surfaces. We propose to model orientation fields of fingerprints by specifying quadratic differentials. Models for all fingerprint classes such as arches, loops, and whorls are laid out. These models are parameterized by a few geometrically interpretable parameters that are invariant under euclidean motions. We demonstrate their ability in adapting to given observed orientation fields, and we compare them to existing models using the fingerprint images of the NIST Special Database 4. We also illustrate that these models allow for extrapolation into unobserved regions. This goes beyond the scope of earlier models for the orientation field as those are restricted to the observed planar fingerprint region. Within the framework of quadratic differentials, we are able to analytically verify Penrose's formula for the singularities on a palm [19]. Potential applications of these models are the use of their parameters as indexes of large fingerprint databases, as well as the definition of intrinsic coordinates for single fingerprint images.

Index Terms—Fingerprint recognition, orientation field, fingerprint modeling, quadratic differentials, rational functions.

1 Introduction

Fingerprints are used in a variety of biometric applications today; see [1] for an overview. Different features of a fingerprint are exploited for identification. Most commonly, local features like minutiae, i.e., endings and bifurcations of ridges, are used for matching; see [2], [3], [4], [5], [6], [7], and [8] for recent advances in this direction. Additionally, global features contain valuable information. They are generally based on the orientation field of the fingerprint, i.e., the undirected field tangential to the fingerprint ridges. Most prominently, the singular points of the orientation fields have been used for classifying fingerprints since the end of the 19th century [9]. Thus, global features not only aid the matching of two fingerprints but are also of great value for finding a fingerprint in a database: They are used to create indexes that make it possible to narrow the search down to fewer candidates, cf. [3], [10], [11], [12], and [13]. The search for such indexes leads to the problem of mathematically modeling those orientation fields. The work of Smith [14], later refined by Mardia et al. [15], was among the first taking on this task. They proposed solutions of algebraic equations that generate different types of fingerprint patterns: whorls, loops, etc. A different class of models based on simple rational complex functions was presented by Sherlock and Monro [16], inspiring the present work. We add to their models global features present across all classes of fingerprints, such as parallel ridges near the joint and circular ridges at the fingertip. These can be modeled naturally using quadratic differentials (QDs). In fact, the models of Sherlock and Monro [16] can be viewed as the simplest QDs respecting the observed singularities. Later, extensions of these models have been proposed; see [17] and [18]. Although adding substantial flexibility, these models do not explicitly take more of the geometrical structure of fingerprints into account. Led by the analytic properties of QDs, we present models honoring the special geometry of fingerprints while keeping the model as simple as possible. Much of the existing work can be understood naturally in the light of QDs. In particular, we show that the famous Penrose formula, cf. [19]

$$\begin{aligned}&\text{number of deltas} + 1\\ &\qquad = \text{number of fingers} + \text{number of loops}\end{aligned} \tag{1}$$

for the ridge structure on an entire palm or sole, translates into a topological assertion about the order of a QD on the respective surface.

Additionally, mathematical models can be used to define intrinsic coordinate systems, i.e., coordinate systems that are defined through the characteristics of the finger and thus do not depend on the specific imprint: They are invariant under euclidean motions. These coordinate systems can in turn be used to intrinsically specify the locations of local features, therefore removing the need to account for euclidean motions when matching two fingerprints. See [20] for a different approach for defining intrinsic coordinates.

With these future applications in mind, we desire several properties for a model of the orientation field to be useful:

• *The authors are with the Institute for Mathematical Stochastics, Georgia Augusta University Goettingen, Maschmuehlenweg 8-10, D-37073 Goettingen, Germany.*
E-mail: {huckeman, hotz, munk}@math.uni-goettingen.de.

Manuscript received 16 Aug. 2006; revised 19 Feb. 2007; accepted 12 Oct. 2007; published online 14 Nov. 2007.
Recommended for acceptance by D. Lopresti.
For information on obtaining reprints of this article, please send e-mail to: tpami@computer.org, and reference IEEECS Log Number TPAMI-0607-0806.
Digital Object Identifier no. 10.1109/TPAMI.2007.70826.

1. *Accuracy.* The model should describe the true orientation field as much as possible.
2. *Invariance under euclidean motions.* Only parameters that are invariant under rotations and translations of the fingerprint image can serve as database indexes.
3. *Robustness against partial observation.* As repeatedly taken fingerprint images do not show the exact same regions, model parameters should be fairly robust against changes of the fingerprint region being observed.
4. *Low dimension.* The number of parameters translates linearly into the amount of memory needed to store each orientation field in a database. Moreover, increasing the number of parameters will most likely decrease the reliability of estimates of single parameters. For both reasons, we want to use as few parameters as possible.
5. *Interpretability.* Parameters should have a geometrical meaning, i.e., they should be identifiable and serve to explain the features of the model.
6. *Predictive power.* It should be possible to predict bad quality, noisy, or unobserved regions, i.e., to interpolate or even extrapolate.

Clearly, reducing the number of parameters will also reduce the accuracy of the model so a good trade-off has to be found. Thus, the main task is to find a simple model that is well adapted to the problem at hand. This work therefore aims at constructing such models, as well as demonstrating their ability to adapt to a given orientation field. Further research is needed to exploit their potential in the applications described above.

As a minimal requirement, the model must encompass the overall ridge flow observed in a fingerprint image. We follow a longstanding biological belief that the dermatoglyphic line structure can be interpreted as lines of tension or, alternatively, as lines of greatest curvature on the embryonic epidermis, cf. [19], [22], [23], and [24]. Hence, in our model, we view the ridge line structure as a family of curves of shortest length in an underlying metrical context. Thus, a model is sought that most simply generates a non-euclidean planar metrical structure whose curves of minimal length correspond to the ridge lines as found in fingerprint images on an observation window and beyond. Obviously, it suffices to consider smooth structures with isolated singularities. Even more simplicity is obtained when considering analytical structures only. As we are dealing with planar images, we can then profit by embedding those into the complex plane and by subsequently employing complex calculus. Generating analytical planar metrics can be taken as the defining property of QDs. For a little more flexibility, we will allow some nonconformal distortion as well. Hence, in our approach, we model the orientation field of a fingerprint image as the field of a "simple" QD under a suitable "not-too-complicated" quasiconformal mapping.

In the following, we will derive such simple QDs, which give rise to geometrically interpretable models for the orientation fields of fingerprints, depending on five real parameters only. Viewing existing models in the light of QDs will help to clarify their mutual relationships. We will then present numerical results for the NIST Special Database 4 [21], demonstrating the accuracy of the proposed models and comparing them to some existing models. This will allow us to argue that we have come up with models for the orientation field using a minimal set of parameters while still giving high fidelity.

The outline of this paper is as follows: in Section 2, we introduce QDs and discuss their basic properties. We show in Section 3 that they indeed represent a flexible tool to model relevant features of orientation fields, such as various types of whorls and loops. Quasiconformal mappings adding some flexibility are discussed in Section 4. Existing models for orientation fields can be viewed in the light of QDs as shown in Section 5. Numerical results validating the described models are given in Section 6. We end with a discussion of how well we were able to meet goals 1-6 above.

2 Quadratic Differentials

QDs originated as a tool for extremal problems for mappings and moduli of complex domains. The ideas were introduced in the 1930s by Grötzsch [25] and by Teichmüller [26]. Today, QDs are an active field of research with various applications mainly in physical sciences. Examples are the study of defects and textures of crystals and $2+1$ gravity [27] and the study of dynamical systems [28]. Among many other contributions, we refer to recent work [29] in the latter area. Reference [30] may serve as a short introduction to the subject, and [31] provides more detail.

On a surface (e.g., a finger), a QD induces a metric, the geodesics of which are given as solutions to a first-order differential equation and are thus easy to compute. As we shall see, QDs can model a wide class of geodesic flows, in particular, the typical flow structures that can be observed in fingerprint images. In our context, the original surface will be a subset of the complex plane on which we observe a planar fingerprint image. The observed ridge flow structure defines a metrical structure that in turn defines a QD. By extending the structures to the entire complex plane and, even more, by assuming that they will have a removable singularity at complex infinity, the surface for our model will be the extended complex plane $\hat{\mathbf{C}} = \mathbf{C} \cup \{\infty\}$, which can be thought of as a two-sphere, called the *Riemann sphere*. Then, the functions defining the QDs are meromorphic on $\hat{\mathbf{C}}$ and, thus, rational.

In this section, along with the investigation of the typical field structures in fingerprint images, we give an introduction to QDs specifically tailored to our purposes. In the Appendix, we provide the fundamental *Normal-Form Theorem*.

2.1 Global and Local Fields in a Fingerprint Image

Fingerprint images are usually classified into four main categories: *right loop* (31.7 percent in the population [32]) and *left loop* (33.8 percent), *whorl* (27.9 percent), *arch* (3.7 percent), and *tented arch* (2.9 percent), cf. Fig. 1.

In the corresponding orientation fields, one observes two structures (see Fig. 2): The *global field* is visible in fingerprints of all classes; it can be viewed as the field of an arch. Near the joint of the third and second phalanx, the global field is parallel to the line along the joint, whereas this field is "hat"-like in the middle, turning into large arcs when proceeding further up to the fingertip.

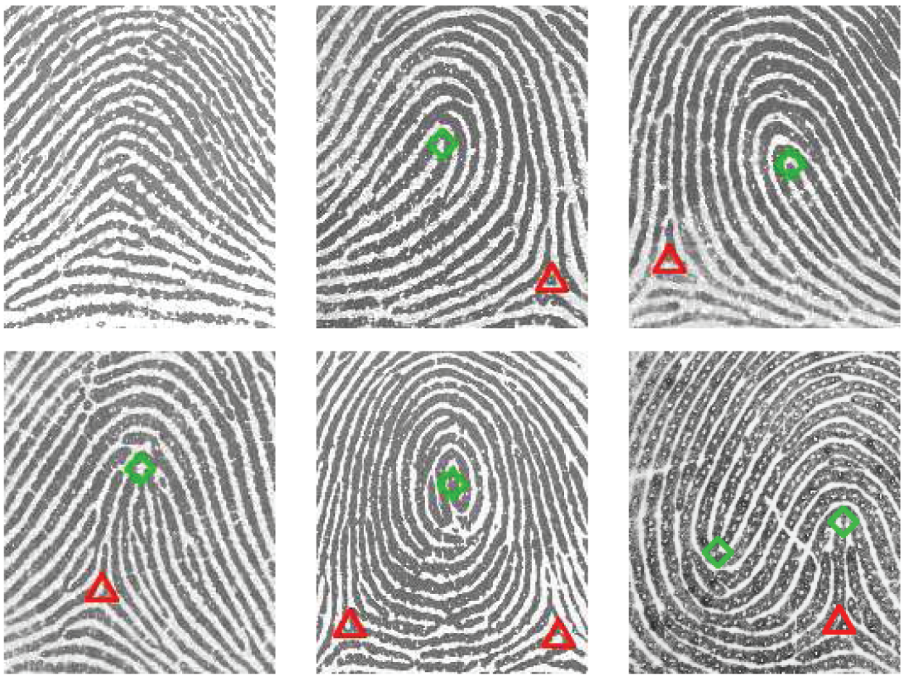

Fig. 1. Fingerprint classes: Top row: arch, left loop, and right loop. Bottom row: tented arch, whorl, and twin-loop. Triangles mark deltas; diamonds mark cores and whorls. Note that there is an invisible delta further to the bottom left of the last image, which actually shows a tented-arch-and-loop rather than a twin-loop. These are based on images from the FVC 2000, Database 2a [34].

The *local field* is generated by the *singular points* of the field: a *delta* occurs at the junction of three lines, a *core* is the endpoint of a single line, and a *whorl* is the center of closed lines, cf. Figs. 1 and 2. As arches feature no singular points, they also bear no local field.

In the first step, we model the field near a singular point. Consider for smooth $\alpha(t) > 0$, $t \in \mathbf{R}$, and $z_0 \in \mathbf{C}$ the differential equation

$$z(t)\,\dot{z}(t)^2 = \alpha(t), \quad z(t_0) = z_0.$$

This has, up to reparameterization, the solution $z(t) = \left(t + z_0^{\frac{3}{2}}\right)^{\frac{2}{3}}$. For varying $z_0 \in \mathbf{C}$, solution curves are depicted in Fig. 3a: a field with a single delta at the origin $(z_0 = 0)$. Similarly, the differential equations

$$\frac{\dot{z}(t)^2}{z(t)} = \alpha(t) \quad \text{and} \quad -\frac{\dot{z}(t)^2}{z(t)^2} = \alpha(t)$$

generate fields with a core and a whorl, respectively, at the origin, as depicted in Figs. 3b and 3c. Since reparameterizations do not change the shape of the solution curves, we abbreviate

$$z\,dz^2 > 0, \quad \frac{dz^2}{z} > 0 \quad \text{and} \quad -\frac{dz^2}{z^2} > 0,$$

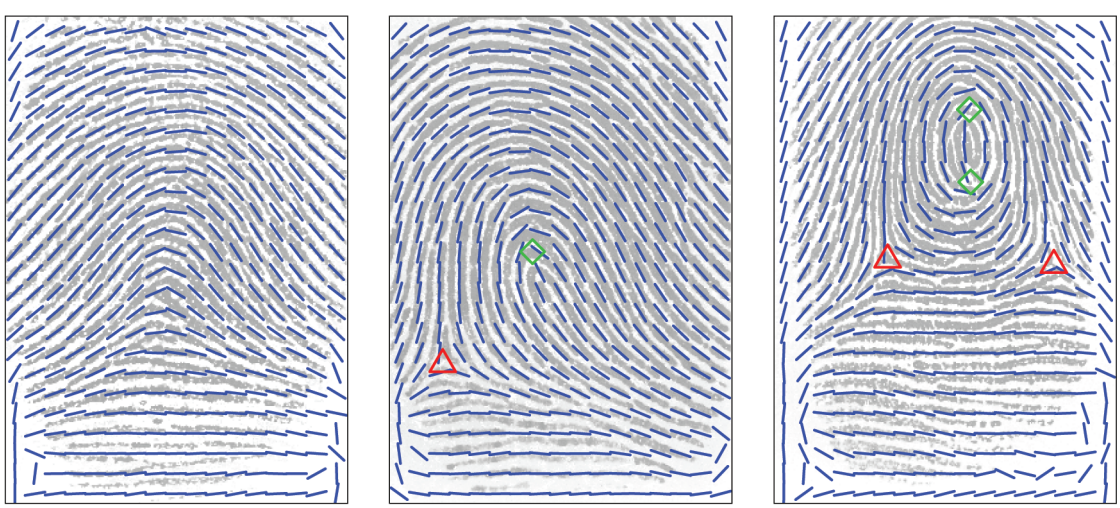

Fig. 2. Orientation fields and singular points extracted from the arch, loop, and whorl (from left to right) in Fig. 1; deltas have been marked by triangles; cores have been marked by diamonds. These are based on images from the FVC 2000, Database 2a [34].

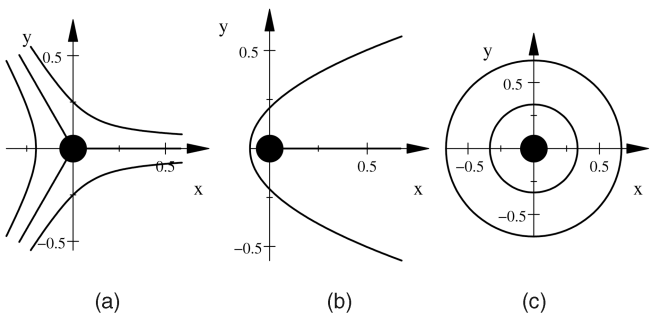

Fig. 3. Fields of QDs generating singular points. (a) $z\,dz^2 > 0$.

characterizing the three types of local fields near singular points (delta, core, and whorl, respectively). Here, (z, dz) can be considered a *line element* of arbitrary length parallel to the trajectory through z; Fig. 2 shows such unit-length line elements on a grid. Specific features may be superimposed by multiplying with a corresponding factor, e.g.,

$$(z-1)\,\frac{dz^2}{z} > 0 \tag{2}$$

models a delta at $z = 1$ and a core at $z = 0$.

More generally, with a rational function $Q(z)$, the condition

$$Q(z)\,dz^2 > 0 \tag{3}$$

defines a unique *orientation field*

$$\mathcal{O} = \left\{ \left(z, \frac{dz^2}{|dz|^2} \right) : Q(z) \neq 0, \infty \right\}$$

on $\mathbf{C}$ except for isolated singular values. The left-hand side of (3) is called a QD and denoted by a Greek letter, say, σ. The squared velocities dz^2 correspond to double angles since orientation fields are not directed. In our model, we assume that the ridge structure of an original fingerprint image is given by an underlying orientation field

$$\mathcal{F} = \left\{ \left(z, \phi(z)^2 \right) : z \in G \right\}$$

defined by a smooth mapping $\phi^2 : G \to S^1$ over an observation window $G \subset \mathbf{C}$ well defined apart from at most isolated singular values. Here, $S^1 = \{z \in \mathbf{C} : |z| = 1\}$ denotes the unit circle.

In Section 4, we shall combine suitable mappings of original fingerprint images with locally isotropic and locally anisotropic distortion. In the language of Complex Analysis, these are *conformal* (angle preserving) and *quasiconformal* (of bounded anisotropy) mappings. Every smooth mapping $f : z \mapsto w = f(z)$ induces a natural transformation of line elements $(z, dz) \mapsto (w, dw)$. The transformed field will be generated by the QD $P(w)\,dw^2 > 0$ if we have the equality

$$Q(z)\,dz^2 = P(w)\,dw^2. \tag{4}$$

(Note that positive factors do not change the field.) We illustrate the conformal case here and treat the general case in Section 4, cf. (14). For a conformal f, we have a *complex derivative* f', i.e., $(w, dw) = (f(z), f'(z)dz)$. Thus, the transformation rule simply is

$$P(w) = \frac{(Q \circ f^{-1})(w)}{\left((f' \circ f^{-1})(w)\right)^2}. \tag{5}$$

Accordingly, under the mapping $z \mapsto \frac{1}{z} = w$, a QD has a continuation to the *Riemann sphere* $\hat{\mathbf{C}}$ given by

$$Q(z)\,dz^2 = Q\left(\frac{1}{w}\right)\frac{dw^2}{w^4}. \tag{6}$$

In particular, this yields the global features of an orientation field "far outside." As an example, consider $\sigma = -(dz/z)^2$ with a whorl at the origin, which also has a whorl at ∞.

2.2 Local Structure of Trajectories

In the preceding section, we illustrated that, for a QD $\sigma = Q(z)\,dz^2$, the condition $\sigma > 0$ is equivalent to a first-order differential equation

$$Q\big(z(t)\big) = \frac{\alpha(t)}{\big(\dot{z}(t)\big)^2}$$

with arbitrary smooth $\alpha(t) > 0$. $\alpha(t)$ only affects the parameterization of the solution curves. Their geometry, however, and, thus, the orientation field $\mathcal{O}$ defined by $\sigma > 0$, is independent of $\alpha(t)$. Thus, we generated typical local features in fingerprint images by QDs with suitable singularities. In fact, the last example of the preceding section demonstrated how local features influence the global field, which is the local field near ∞. In this section, we investigate the geometry of solution curves more closely in order to simultaneously and more broadly model the global field of fingerprint images in Section 3. This geometry is determined by the singular points and some leading coefficients only. In particular, singularities of negative even order will go into our global models. Also, the *residues*, as discussed below, will shed further light on the local field of a whorl.

Every (maximal) solution curve of the orientation field defined by $\sigma > 0$ is called a *trajectory* of σ. Apart from reparameterization, every trajectory can be obtained through the integration and inversion of

$$t = \int_{z(0)}^{z(t)} \sqrt{Q(z)}\,dz. \tag{7}$$

According to the Normal-Form Theorem (see the Appendix), the local structure of trajectories near z_0 is determined by the *order* $n = n(z_0)$ of Q at z_0 and the square of the *residue* (the coefficient a_{-2} if present) from a Laurent power series expansion:

$$Q(z) = \sum_{k=n}^{\infty} a_k (z - z_0)^k.$$

Points of nonzero order are called *singular points*, points of negative order are called *poles* of order $|n|$, and points of positive order are *zeros* of order n.

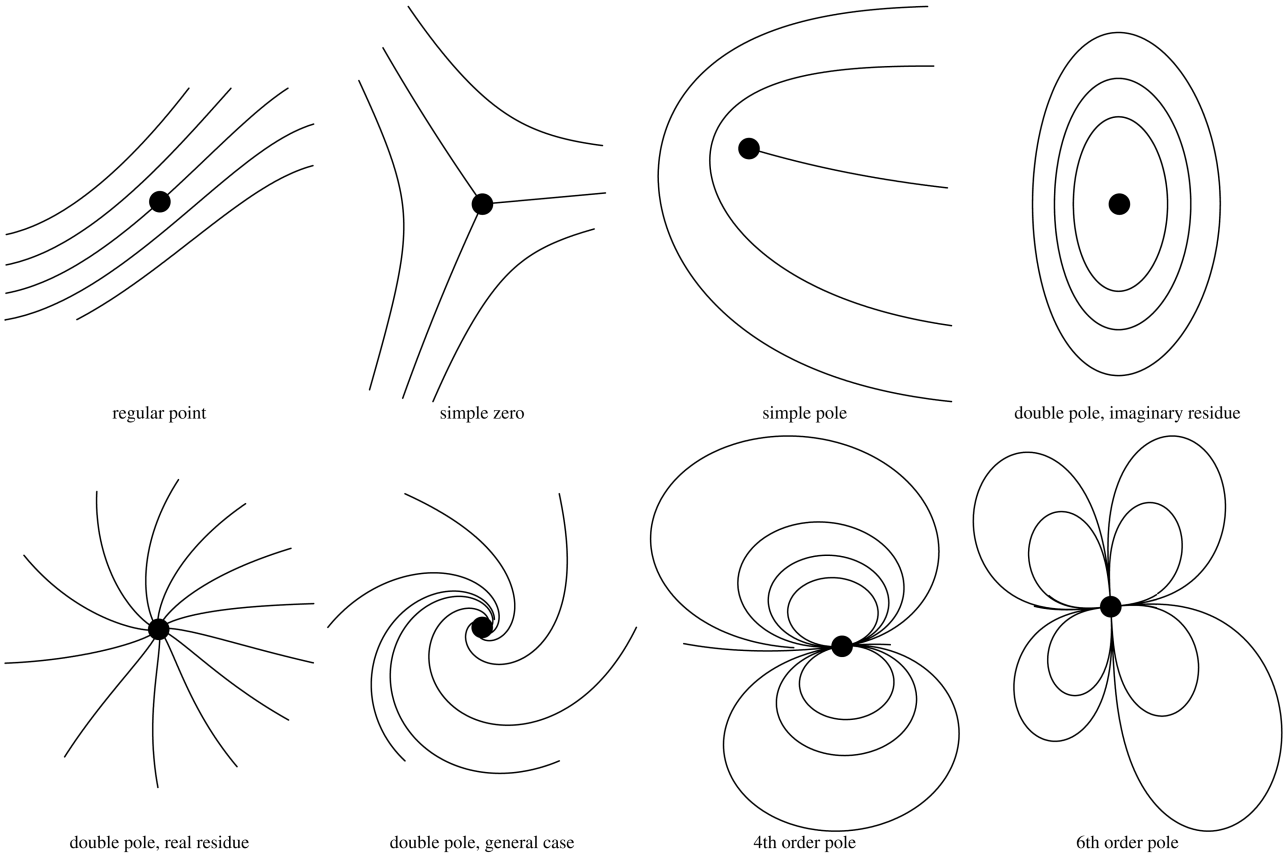

Fig. 4. Local trajectory structure near a point z_0 of order $n \in \mathbf{Z}$ Going from left to right and from top to bottom, the different cases for $n = 0, 1, -1$, -2 $(a_2^2 < 0)$, -2 $(a_2^2 > 0)$, -2 $(a_2^2 \notin \mathbf{R})$, -4, and -6 are illustrated.

Thus, as a consequence of the Normal-Form Theorem and (7), we have the following local trajectory structure around a point z_0 of order n, cf. Fig. 4:

- In case of $n = 0$, there is exactly one trajectory through z_0.
- In case of $n > 0$, there are exactly $n + 2$ trajectories emanating from z_0 at angles of $\frac{2\pi}{n+2}$.
- In case of $n = -1$, there is exactly one trajectory emanating from z_0.
- In case of $n = -2$, all trajectories are conformal images of
  - concentric circles about z_0 if $(a_{-2})^2 < 0$,
  - radial rays emanating from z_0 if $(a_{-2})^2 > 0$, and
  - logarithmic spirals ending at z_0 for any other a_{-2}.
- In case of $n < -2$, all trajectories end at z_0 coming in from $|n| - 2$ limit directions at angles of $\frac{2\pi}{|n|-2}$.

If existent, the sum over the orders of all singular points is called the *order* of the QD. This corresponds to the topological genus of the Riemann surface. As is clear from (6), all QDs on the Riemann sphere have order -4, whereas on a torus, their order is 0.

3 Quadratic Differentials for Fingerprint-Like Ridge Flows

In view of the behavior of a QD near ∞ and the above classification of the local trajectory structure of QDs, we model the global field of a fingerprint image by a QD of type

$$\sigma_{2n} := \frac{dz^2}{(z^2 - R^2)^{2n}}, \tag{8}$$

with suitable $n \in \mathbf{N}$, $R > 0$. This QD has poles at $\pm R$ of order $2n$, and $z = \infty$ is a point of order $2n - 4$. The real axis with the poles removed is a trajectory. Fig. 5 depicts the flow generated by σ_2 and σ_4. Note that σ_4 accurately simulates

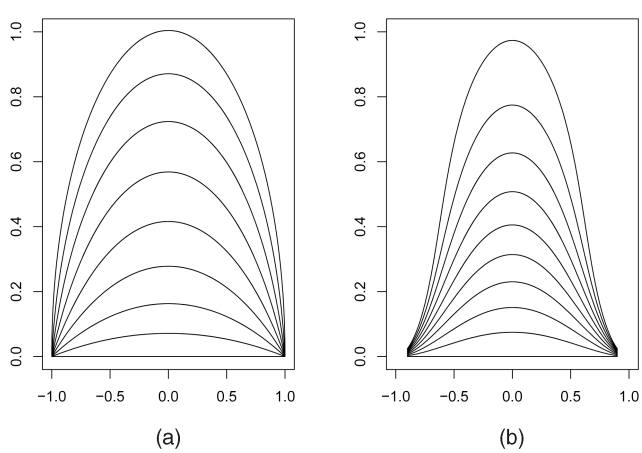

Fig. 5. (a) σ_2 has double poles at the two lower corners with positive residue and is regular at ∞. (b) σ_4 has fourth-order poles at the two lower corners and a double zero at ∞.

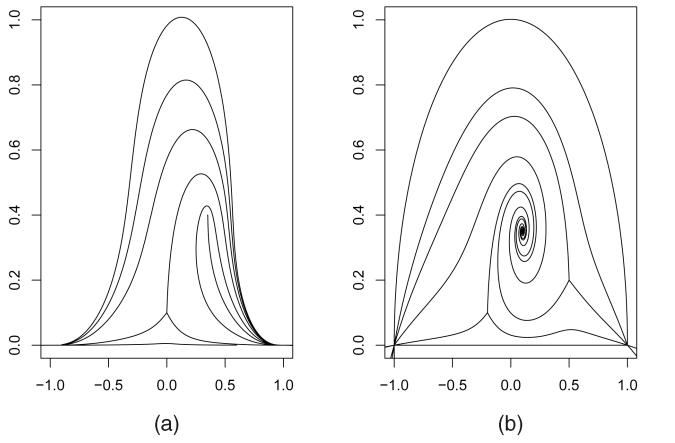

Fig. 6. (a) Model $\sigma_{basic,6}$ for a single core. (b) Model σ_{circ} for a whorl. The residue is not purely imaginary.

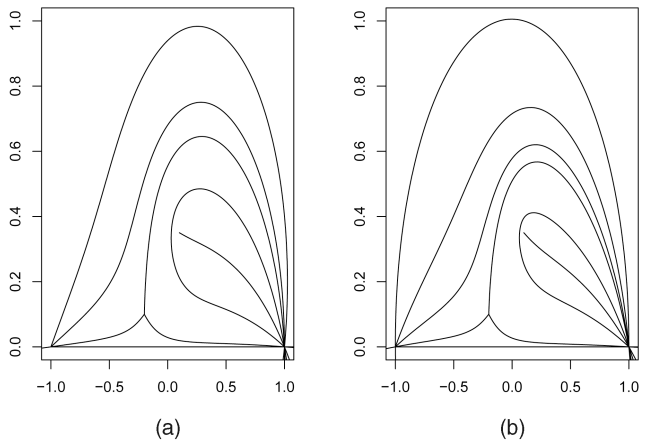

Fig. 7. Pole and zero at the same position. (a) $\sigma_{basic,2}$, i.e., no symmetry with respect to the unit circle. (b) Including symmetry, σ_{circ}.

the varying curvature of the ridge lines of "towering hats" found as the "outer field" in most fingerprints.

Since the local field is generated by the singular points, in the terminology of QDs, *deltas* correspond to simple zeros, *cores* correspond to simple poles, and *whorls* to second-order poles with (almost) purely imaginary residue, cf. Figs. 1, 2, 3, and 4.

In order to model the local structure of the orientation field, we generalize (2) and introduce

$$Q_{p_1,p_2,q_1,q_2,R}(z) := \frac{(z - Rq_1)(z - Rq_2)}{(z - Rp_1)(z - Rp_2)}, \tag{9}$$

again for $R > 0$ and p_i, $q_i \in \mathbf{C}$, with $0 < |p_i|, |q_i| < 1$, $\mathbf{Re}(p_i)$, $\mathbf{Re}(q_i) > 0$, and $i = 1, 2$. Then, the QD $Q_{p_1,p_2,q_1,q_2,R}(z)dz^2$ generates deltas at Rq_1 and Rq_2, as well as cores at Rp_1 and Rp_2. If there is only one delta and one core present, we have $p_2 = q_2$, for example. In case of two deltas and a whorl, we would have $p_1 = p_2$. This QD, however, is no longer necessarily positive along the real axis. In order to ensure positivity, we include the complex conjugate. Merging the local with the global field, call

$$\sigma_{basic,2n} := \sigma_{2n}\, Q_{p_1,p_2,q_1,q_2,R}(z)\, Q_{\overline{p}_1,\overline{p}_2,\overline{q}_1,\overline{q}_2,R}(z) \tag{10}$$

the *basic model*. Indeed, the trajectory structure of this QD is symmetric to the real axis, so the real axis (with the poles removed) itself is a trajectory. Note that $\sigma_{basic,2n}$ inherits the global properties of σ_{2n} as the orders of its other factors sum to zero. Thus, there is a singularity of order $4n - 4$ at complex infinity defining the global field (cf. (6)).

In case of $n = 1$, the QD σ_2 is also symmetric with respect to the R-circle taken about the origin. With this in mind, call

$$\sigma_{circ} := \sigma_{basic,2}\, Q_{1/p_1,1/p_2,1/q_1,1/q_2,1/R}(z) \cdot Q_{1/\overline{p}_1,1/\overline{p}_2,1/\overline{q}_1,1/\overline{q}_2,1/R}(z) \tag{11}$$

the *circular model*. The trajectory structure of this QD is then also symmetric with respect to the R-circle about the origin. Fig. 6 shows typical QDs for the basic model and the circular model. The symmetry condition for the circular model yields nearly circular ridge lines as are typical around the fingertip. Fig. 7 illustrates the subtle difference between the circular and basic model for $2n = 2$, i.e., $n = 1$.

The QDs defined so far model the orientation field of a fingerprint by imposing a symmetry with respect to the real line. Although this results in realistic models for such a field above the real axis (on the upper half-plane), they are unrealistic and invalid below the real axis (on the lower half-plane). Since the real axis models the field close to and parallel to the joint, we therefore extend our models to predict orientations parallel to the real axis on the lower half-plane (i.e., $Q(z) = 1$ for $\mathbf{Im}(z) < 0$). This extension is continuous since the real axis itself is a trajectory of the QD due to the symmetry condition. As the most interesting part of the fingerprint is above the real axis, we will not elaborate further on this point.

We are now in a position to verify Penrose's formula (1). Penrose arrived at it using topological arguments: He mapped the entire palm to the interior of a circle such that all lines exiting are perpendicular to the boundary, whereas fingernails and the wrist of the hand are parallel to the boundary. He then determined the necessary relationship between cores and deltas for such a mapping to be possible; see [19].

We will deduce Penrose's formula by induction over the number of fingers F. Recall that the order of a QD on the sphere is -4, cf. Section 2. As a finger is represented only by a half-sphere (with a field parallel to the equator), the corresponding QD's order is -2. Hence, for a single finger, we have

$$D - L - 2 = -2, \tag{12}$$

where D denotes the number of deltas observed, L is the number of loops (whorls count as two loops), and the term -2 on the left represents an unobserved whorl that results from continuing the field around the nail of the finger. This is precisely the Penrose formula for a single finger (i.e., for $F = 1$):

$$D + 1 = L + F. \tag{13}$$

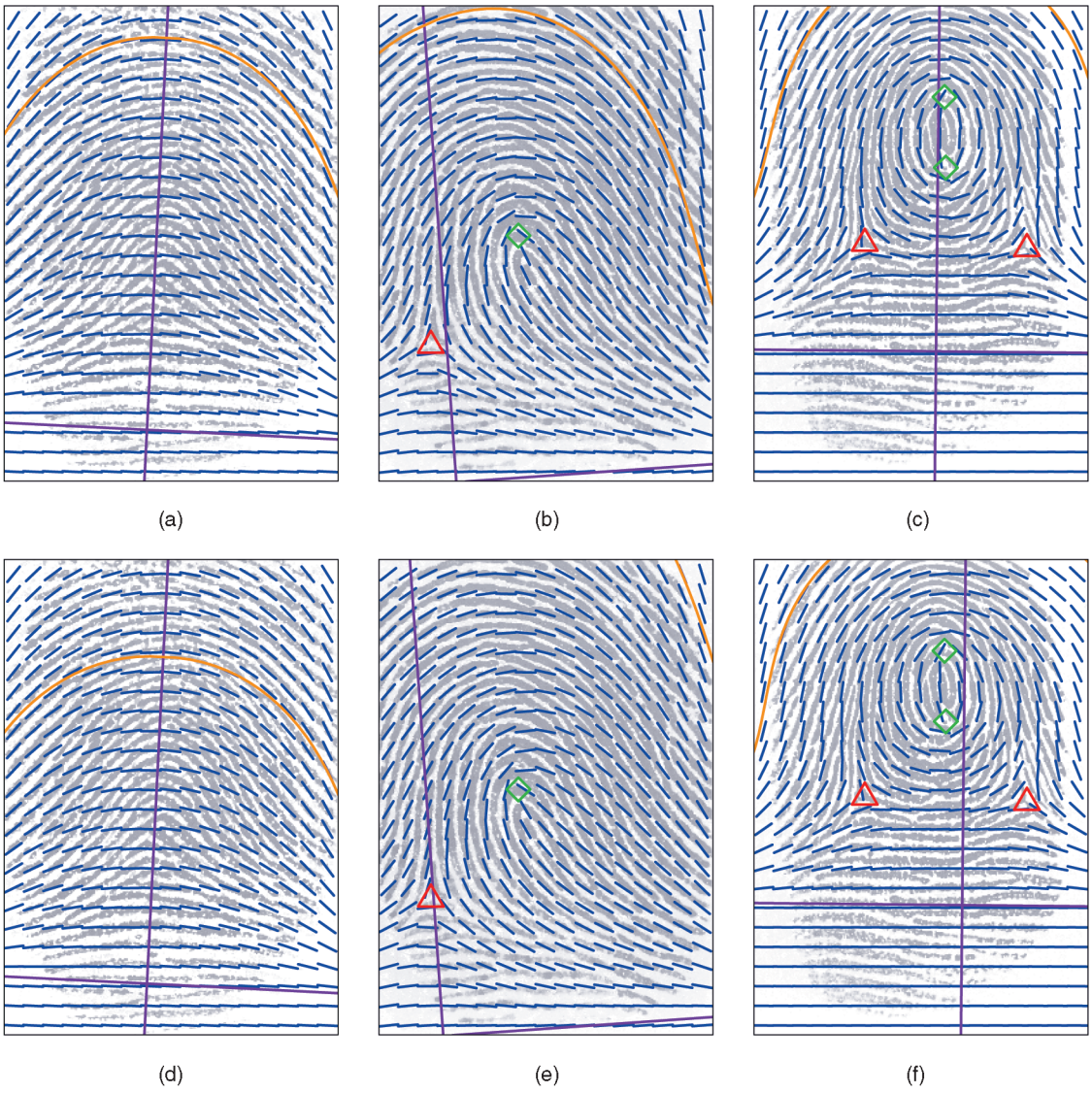

Fig. 8. Models $\sigma_{basic,4}$ (first row) and $\sigma_{basic,6}$ (second row). (a) and (d) Applied to an arch. (b) and (e) Applied to a loop. (c) and (f) Applied to a whorl. Deltas have been marked by triangles, cores have been marked by diamonds, violet lines show corresponding coordinate axes, and orange lines give the trajectories through cRi. These are based on images from the FVC 2000, Database 2a [34].

It is easily seen that adding another finger results in observing one more delta than loop, proving Penrose's formula.

4 Mapping from a Fingerprint Image to the Domain of a Quadratic Differential

In this section, we assume that

$$H := \{w = u + iv : u = 1, \ldots, M, v = 1, \ldots, N\},$$

$H \subset \mathbf{C}$, is a given original fingerprint image being M pixels wide and N pixels high. We assume the *original orientation field*

$$\mathcal{O} = \{(w, dw^2) : w \in H \setminus D, dw \in S^1 \subset \mathbf{C}\},$$

to be known (see Section 6 for extracting it from a fingerprint image), where $D \subset H$ denotes the set of singular values (i.e., cores, deltas, and whorls) of the observed finger.

Clearly, this orientation field first needs to be transformed before it can reasonably be described by the QDs specified above, e.g., a change of coordinates is inevitable, cf. Figs. 8 and 9 showing such transformed coordinate systems. A suitable smooth mapping $f : G \to H$, $G \subset \mathbf{C}$, will thus map from the z-plane into the observation window, in which the observed orientation field is approximated by the image under f of an orientation field defined by a QD $\sigma = Q(z)dz^2 > 0$ in G as described above. The line element $dz = dx + idy$ is mapped to the line element $dw = du + idv$ via

$$\begin{pmatrix} \frac{\partial \mathbf{Re}(f)}{\partial x} & \frac{\partial \mathbf{Re}(f)}{\partial y} \\ \frac{\partial \mathbf{Im}(f)}{\partial x} & \frac{\partial \mathbf{Im}(f)}{\partial y} \end{pmatrix} \begin{pmatrix} dx \\ dy \end{pmatrix} = \begin{pmatrix} du \\ dv \end{pmatrix}, \tag{14}$$

cf. (5) for the special case of conformal f.

We assume that the mapping f is the composition of several mappings as follows: By necessity, a (conformal) euclidean motion has to be included:

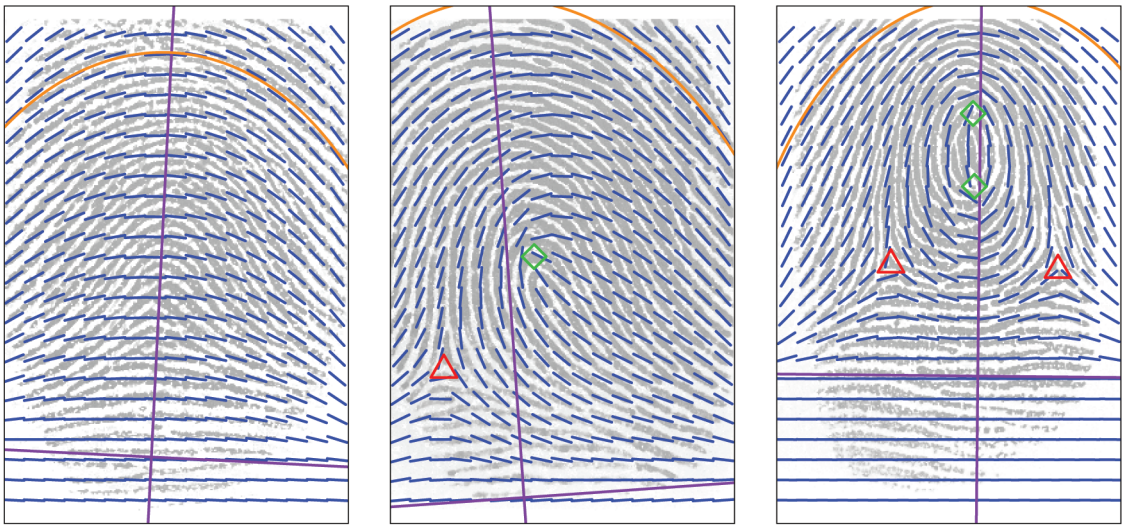

Fig. 9. Model σ_{circ} applied to an arch, a loop, and a whorl (from left to right). Deltas have been marked by triangles, cores have been marked by diamonds, violet lines show the corresponding coordinate axes, and orange lines give the preimages of the "circles of symmetry." These are based on images from the FVC 2000, Database 2a [34].

$$E_{\theta,m} : w \to w' = e^{-i\theta}(w - m),$$

where $\theta \in [0, 2\pi)$ and $m \in \mathbf{C}$ correspond to the inclination of the proposed "symmetry axis," the preimage of the real axis in the z-plane (roughly the joint of the third and second phalanxes), and the preimage of the origin (roughly the center of the joint), respectively, cf. Figs. 8 and 9. Also, in particular, in view of the circular model, we will use an affine mapping (the most simple nontrivial quasiconformal mapping)

$$L_c : w' = u' + iv' \to z = u' + icv',$$

for some suitable $c > 0$, turning the circle into an ellipse, cf. Fig. 9. In fact, c can be viewed as a measure of thickness of the particular finger: the ratio of its length and width. More mappings could be included, e.g., an affine map compensating for a distortion stemming from a specific scanning device.

In this paper, we use the mapping

$$F_{c,\theta,m} := f^{-1} = L_c \circ E_{\theta,m} : w \to z,$$

determined by four real parameters (recall that $m \in \mathbf{C}$). As all of the QDs proposed above only depend on R (assuming the singular points to be known), each orientation field is uniquely determined by just five real parameters. These parameters can be obtained by numerical optimization when fitting the model to real data, cf. Section 6.

5 Comparison to Existing Models

Possibly the first mathematical model, which aimed at verifying the biological findings in [23], has been stated by Smith [14]. When translated into the framework laid out above, it models the ridge line structure near a singular point using the nonmeromorphic QD

$$\big(z - z_0 - \alpha i|z - z_0|\big)^{2\alpha} dz^2 > 0,$$

with $\alpha = 1$ for a delta at z_0 and $\alpha = -1$ for a core at z_0. This model has been extended using higher order nonmeromorphic terms for all local structure elements such as cores, whorls, etc., by Mardia et al. [15], involving a larger number of parameters not directly interpretable. Sherlock and Monro [16] were first in proposing a model that in our framework translates into a meromorphic QD. They suggest simply to use

$$\sigma(z) = \beta\, \frac{z - d}{z - c}\, dz^2, \tag{15}$$

for a loop with a core at c and a delta at d (and accordingly for the other classes); $\beta \in S^1$ is the orientation at ∞ that allows for rotations. This model clearly is too simplistic but has served as an inspiration not only for us but also for several other authors.

To make the model more adaptive, Vizcaya and Gerhardt [17] propose (again for a loop)

$$\arg(Q(z)) = g_d(\arg(z - d)) - g_c(\arg(z - c)), \tag{16}$$

with piecewise linear functions g_c, $g_d : S^1 \to S^1$. Similarly, Zhou and Gu [33] suggest

$$\sigma(z) = \frac{1}{f(z)}\, \frac{z - d}{z - c}\, dz^2, \tag{17}$$

with some (complex) polynomial f of order 6. Gu et al. [18] propose

$$\begin{aligned}\sigma(z) = \Big(& w(|z - c|)(z - c) \\ & + w(|z - d|)\, \frac{1}{z - d} \\ & + p_1\big(\mathbf{Re}(z), \mathbf{Im}(z)\big) \\ & + i\, p_2\big(\mathbf{Re}(z), \mathbf{Im}(z)\big)\Big)^{-1} dz^2,\end{aligned} \tag{18}$$

with weights w depending on the distance, and p_1 and p_2 being some real-valued polynomials of order 4 in $\mathbf{Re}(z)$ and $\mathbf{Im}(z)$. We point out that, in general, only the models of

TABLE 1
Number of Parameters Used[1]

model	number of (real) parameters
Sherlock & Monro [16]	1
Vizcaya & Gerhardt [17]	$10K$
Zhou & Gu [33]	13
Gu et al. [18]	$K + 32$
newly proposed models	5

[1] *K denotes the number of singular points; the locations of the singular points have not been counted as parameters as they are extracted from the image.*

Sherlock and Monro [16] and of Zhou and Gu [33] define QDs as introduced in Section 2.

The difference between these generalizations of (15) and our approach is clear: We aim at modeling the orientation field on a large scale, i.e., its global features, using properties of orientation fields that are specific to fingerprints, leading to just a few geometrically meaningful parameters. These provide global information about a fingerprint's orientation field. Note that since we model the euclidean motion explicitly, our parameters should not vary much if a second imprint of the same finger is taken. In contrast, due to the high number of parameters (see Table 1 for a comparison of the numbers of parameters used in the different models), the models (16)-(18) should be able to adapt to the orientation field almost perfectly. However, as a consequence of the largely increased flexibility of those locally adapting models, artifacts may be created. For example, any zero of the polynomial f in the model of Zhou and Gu [33] will create a pole for the QD σ, i.e., a singular point in the orientation field. Hence, the parameters of those existing models may vary strongly when a second fingerprint image is taken, showing a different region (cf. requirement 3 in Section 1). Furthermore, those models are only valid for the region observed; hence, they cannot be used for predicting the orientation field outside that region, i.e., for interpolation or extrapolation (requirement 6 in Section 1). The QDs proposed above, on the other hand, completely model a fingerprint using only a few parameters and thereby can be used for prediction even outside of the observed region.

6 Numerical Results and Validation on a Database

6.1 Illustrating Examples

We illustrate the models described above by applying them to three fingerprints: one arch, one loop, and one whorl, taken with kind permission from Database 2a of the Fingerprint Verification Competition [34] (as distributed with [1]). We do not show the results for a tented arch since it can be viewed as a special case of a loop, as in the original classification by Galton [9]. For all three fingerprints, the original orientation field has been computed using the methods proposed by Bazen and Gerez [35], as well as smoothed with a Gaussian kernel; see Fig. 2. Approximating basic models for these fingerprints are shown in Fig. 8, $\sigma_{basic,4}$ in Figs. 8a, 8b, and 8c and $\sigma_{basic,6}$ in Figs. 8d, 8e, and 8f, where the preimages of the axes have been drawn as violet lines. Fig. 9 shows approximating circular models where, additionally, the preimages of the "circles of symmetry" have been drawn in orange. The models' parameters have been chosen such as to minimize the deviation of the model from the "true" orientation field (cf. Section 6.2). Again, the preimages of the coordinate axes and a sample trajectory starting from the preimage of cRi have been drawn as violet and orange lines. Note that the field below the preimage of the real axis is parallel to the real axis as discussed above; this is most clearly visible for the whorl.

The figures clearly demonstrate the ability of the proposed models to capture the main characteristics of the fingers' orientation fields. As expected from the small number of parameters, they cannot fit the original orientation field perfectly; however, they differ from it only on a local scale. Note that the field is especially well adapted where the influence of the singularities is strong. Thus, loops and whorls can be fitted with a high degree of precision. Fitting arches is more difficult; further research will be necessary to model the distortion created at the center of an arch. Although each of the three models defines for each example finger a different coordinate system, any single model could—at least in principle—be used to define consistent intrinsic coordinates.

Fig. 10 illustrates the predictive power of these models for two examples: an arch where a large portion in the middle has not been observed but predicted using model $\sigma_{basic,4}$ and a whorl where the upper left part has not been observed but predicted using model σ_{circ}. Figs. 10a and 10d show the fingerprint image without the unobserved part (this could also be automatically cut out because of poor quality, e.g., low contrast), together with the original orientation field in the observed region. Figs. 10b and 10e show the model fitted to this field and extrapolated into the unobserved region. Figs. 10c and 10f show the field predicted by the model in blue on top of the original orientation field of the whole fingerprint image in orange. Clearly, the extrapolated fields agree quite well with the true original orientation field, considering the amount of data given. As noted earlier, the accuracy is again much higher where singularities influence the field strongly.

6.2 Validation on the NIST 4 Special Database and Comparison with Other Models

Using the NIST Special Database 4 [21], we measured the accuracy of the new models described above when applied to a large number of fingerprints. We also compared them with the models in [16] and [33] in their ability to adapt to a given orientation field. From the 4,000 images in that database, we analyzed 3,159 images, where all singularities were visible and could be reliably extracted; recall that all models considered require knowledge of the locations of all singularities. For the extraction of the "true" orientation field and singularities, we again used the algorithm described in [35]; 1,103 images showed no core (arches), 1,546 showed one core (loops and tented arches), and 510 showed two cores (whorls). We then fitted all mentioned models automatically to the extracted orientation field. To measure the quality of the fit, we computed the average difference between the extracted orientation field and the

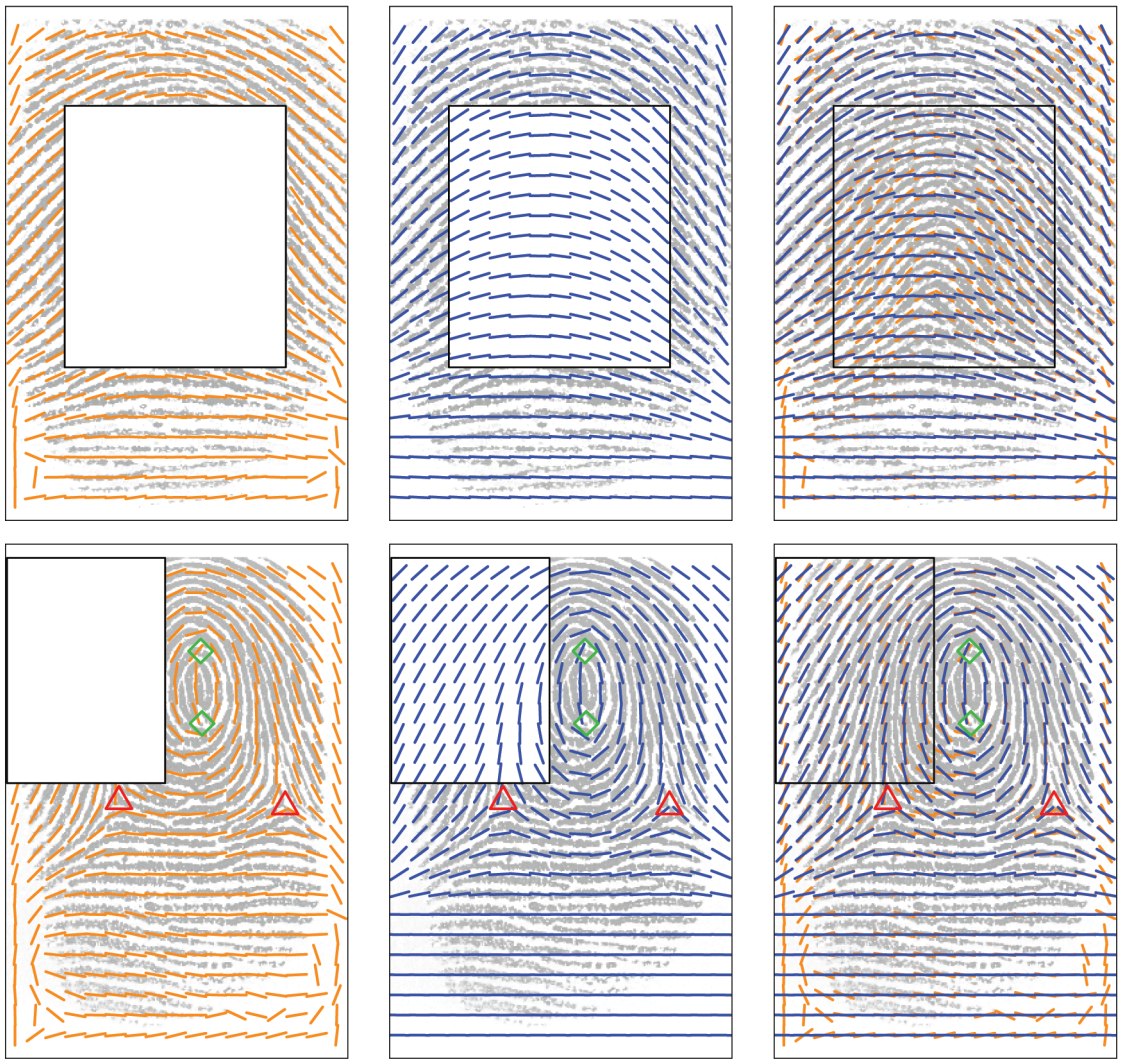

Fig. 10. Prediction of an arch using model $\sigma_{basic,4}$ (first row) and of a whorl using model σ_{circ} (second row). (a) and (d) Fingerprint where some part has not been observed with its orientation field in orange. (b) and (e) Model in blue, fitted to the observed part and extrapolated to the unobserved part. (c) and (f) Model in blue on top of the original orientation field of the whole fingerprint image in orange. These are based on images from the FVC 2000, Database 2a [34].

fitted orientation field in degrees, where the average has been computed in the foreground only. The models in [16] and [33] were fitted by least squares in the foreground. Fitting the other models was achieved by numerically optimizing their accuracy as measured by the average difference; we used a general-purpose minimizer [36] to find the optimal parameters.

Table 2 gives some basic statistics over those average differences collected over all images, as well as for the images split up into the three classes above; more details can be gathered from Fig. 11, showing the respective cumulative distribution functions. Direct comparisons of all models with the model of Sherlock and Monro [16] are shown in Table 3, where the percentage of images is reported for which a model outperformed (in the sense of having a smaller average difference) the model in [16]. Similarly, Table 4 gives the results of a direct comparison with the model of Zhou and Gu [33]. Recall that by definition models, $\sigma_{basic,2}$ and σ_{circ} agree when no singularities are present, i.e., for arches.

These tables show clearly that the proposed models are very much able to model the orientation fields of fingerprints in all fingerprint classes. One readily observes that these models fit better relative to the two existing models the fewer singularities that are present; for whorls, the fit of the model

TABLE 2
Median of Average Differences[1]

model	all images	no core	one	two
Sherlock et al. [16]	22.8	28.0	22.1	14.0
Zhou & Gu [33]	13.4	17.0	12.8	8.3
$\sigma_{basic,2}$	11.3	12.6	11.0	8.5
$\sigma_{basic,4}$	10.4	11.9	10.0	8.2
$\sigma_{basic,6}$	10.5	11.7	9.8	9.0
σ_{circ}	10.5	12.6	9.8	8.0

[1] *For each image in the NIST Special Database 4 [21] and each model (rows), the average difference in degrees between the "true" orientation field and the fit of the model has been computed; the columns give the median of these average differences summarized over all images of the database, as well as for all images showing no core, one core, or two cores, respectively, cf. Fig. 11.*

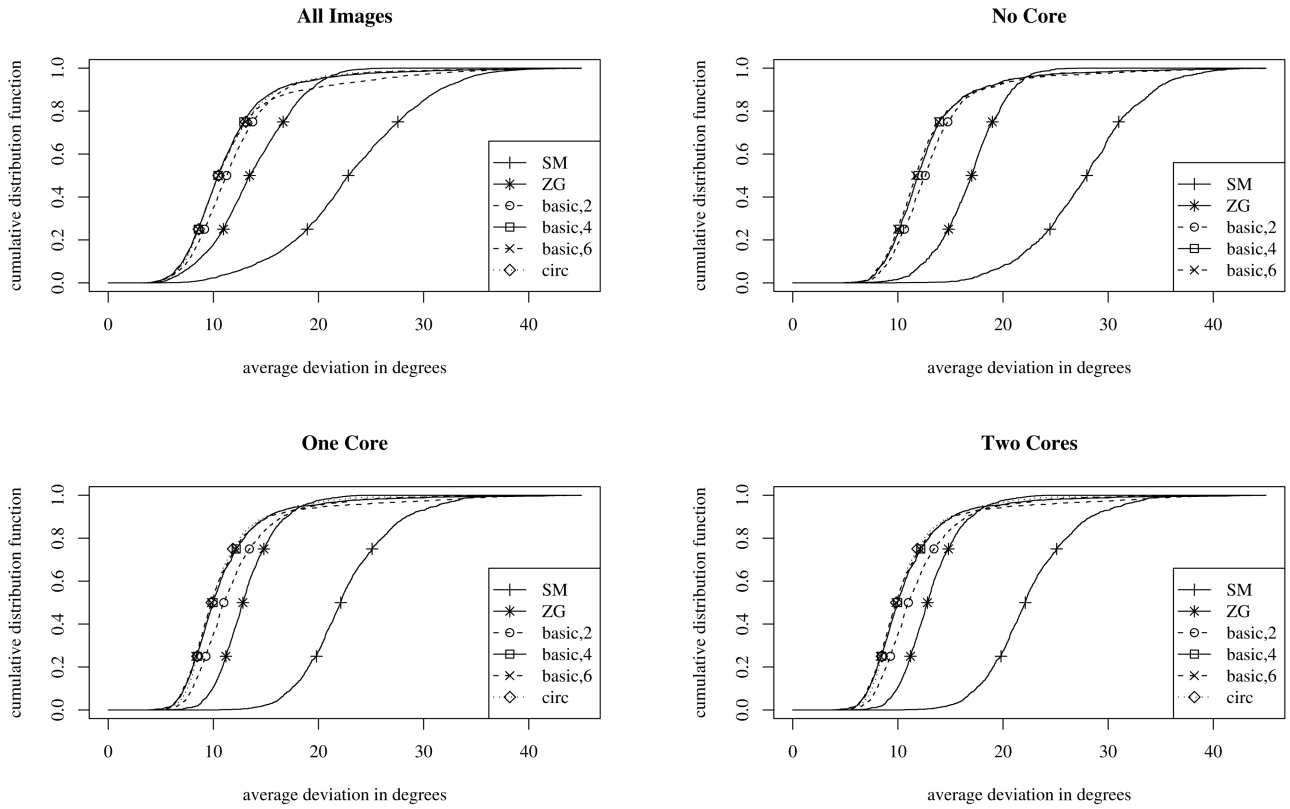

Fig. 11. For each image in the NIST Special Database 4 [21] and each model, the average difference in degrees between the "true" orientation field and the fit of the model has been computed. The figures give the cumulative distribution functions of these average differences summarized over all images of the database, as well as for all images showing no core, one core, or two cores, respectively. The median, lower, and upper quartiles have been marked (recall that models $\sigma_{basic,2}$ and σ_{circ} are equivalent for arches).

of Zhou and Gu [33] is seen as good as that of the proposed models. This is not surprising: Our aim was to model the global field well; the more singularities there are, however, the more the orientation field is dominated by its local field generated by those singularities.

7 Discussion

Returning to aims 1-6 that we set ourselves in Section 1, we will now assess what we have achieved:

- *Aim 1.* Comparing the fit of our models with the fit of other existing models, we see that they do very well except for a small number of images for which the rotation of the field could not be reliably estimated. Given the small number of parameters our models use, we deem this a remarkable achievement. Apparently, these models are able to capture the behavior of the global field. Nonetheless, further increasing our models' accuracy while keeping their attractive properties remains a challenging task, especially so for arches. We realize though that some of the existing models might be more flexible in general, as has been discussed in Section 5, and hence, their ability to adapt could be higher. In particular, they may be able to model local distortions, which may result from differing pressures put on a sensor like an FTIR sensor. However, this is a feature of the sensor: A touchless sensor does not give rise to such distortions. Moreover, the increased flexibility of those models comes at the

TABLE 3
Comparison[1] with the model of Sherlock and Monro [16]

model	all images	no core	one core	two cores
Zhou & Gu	100.0 %	100.0 %	100.0 %	100.0 %
$\sigma_{basic,2}$	95.6 %	97.6 %	96.1 %	89.8 %
$\sigma_{basic,4}$	95.5 %	97.7 %	96.4 %	88.0 %
$\sigma_{basic,6}$	91.7 %	96.2 %	94.6 %	72.9 %
σ_{circ}	96.6 %	97.6 %	98.3 %	89.4 %

[1] *For each image in the NIST Special Database 4 [21], each model's fit (rows) has been compared to the fit of the model of Sherlock and Monro [16]; the numbers give the percentage of images (second column: of all images, third column: of those images showing no core, etc.) where the model mentioned outperformed the model of Sherlock and Monro [16].*

TABLE 4
Comparison[1] with the model of Zhou and Gu [33]

model	all images	no core	one core	two cores
$\sigma_{basic,2}$	71.7 %	87.3 %	67.5 %	50.6 %
$\sigma_{basic,4}$	77.5 %	88.6 %	77.7 %	52.5 %
$\sigma_{basic,6}$	77.0 %	88.5 %	79.1 %	45.7 %
σ_{circ}	80.5 %	87.3 %	83.4 %	56.7 %

[1] *For each image in the NIST Special Database 4 [21], each model's fit (rows) has been compared to the fit of the model of Zhou and Gu [33]; the numbers give the percentage of images (second column: of all images, third column: of those images showing no core, etc.) where the model mentioned outperformed the model of Zhou and Gu [33].*

price of no longer generalizing well, i.e., these models cannot be used for indexing.

- *Aims 2-5*. The parameters of our models describing the orientation field are interpretable, having a clear geometric meaning. Since accounting for euclidean motions is inevitable, we only use two real parameters, R and c, to adapt to the field. If one views these as the parameters scaling the *width* and *thickness* of the finger, one can say that we arrived at a minimal set of five (real) parameters to describe such orientation fields. Given their geometric interpretation, these parameters should also be robust against partial observation, although this needs to be verified empirically in future studies.
- *Aim 6*. The models described can be used for interpolation and extrapolation. However, the predictions cannot be more precise than the accuracy of the fit to the observed field (cf. aim 1 above). In particular, a substantial part of the fingerprint image has to be observed in sufficient quality in order to model noisy or unobserved parts. Further research is needed to fully exploit the predictive abilities of these models.

In summary, we can say that we succeeded in finding simple models for orientation fields of fingerprints that are able to describe all fingerprint classes reasonably well. It would be interesting to see how well the parameters thus obtained can be used as indexes in a fingerprint database. To this end, an empirical study of the parameters' robustness and of their discriminatory power would be a natural next step.

Appendix

The Normal-Form Theorem

Suppose that a QD $\sigma = Q(z)dz^2$ is locally near $z = z_0$ given by the Laurent power series expansion:

$$Q(z) = \sum_{k=n}^{\infty} a_k (z - z_0)^k.$$

Then, the *Normal-Form Theorem* (cf. e.g., [30, p. 211]) states that there is always a conformal map $f(z) = w$, $f(z_0) = 0$, from a neighborhood U of z_0 to neighborhood V of the origin such that for $z \in U$ and $w = f(z) \in V$

- $Q(z)dz^2 = w^n\, dw^2$ for $n \neq -2m$, $m = 1, 2, \ldots$,
- $Q(z)dz^2 = a_{-2} w^2\, dw^2$ for $n = -2$, and
- $Q(z)dz^2 = \left(w^{\frac{n}{2}} + \frac{\sqrt{a_{-2}}}{w}\right)^2 dw^2$ for $n = -4, -6, \ldots$.

$\sqrt{a_{-2}}$ is called the *residue* of σ at $z = z_0$; it is uniquely determined up to the sign.

Acknowledgments

The authors are indebted to the editor and the reviewers for their support and for their helpful comments from which this article has benefited much. They thank their colleagues Preda Mihailescu and Krzysztof Mieloch for fruitful discussions and technological support. Stephan Huckemann gratefully acknowledges the support of Volkswagen Stiftung and DFG Grant MU 1230/10-1; Thomas Hotz gratefully acknowledges support of the DFG Research Training Group 1023 "Identification in Mathematical Models: Synergy of Stochastic and Numerical Methods."

References

[1] D. Maltoni, D. Maio, A.K. Jain, and S. Prabhakar, *Handbook of Fingerprint Recognition*. Springer, 2003.
[2] M. Tico and P. Kuosmanen, "Fingerprint Matching Using an Orientation-Based Minutia Descriptor," *IEEE Trans. Pattern Analysis and Machine Intelligence*, vol. 25, no. 8, pp. 1009-1014, Aug. 2003.
[3] B. Bhanu and X. Tan, "Fingerprint Indexing Based on Novel Features of Minutiae Triplets," *IEEE Trans. Pattern Analysis and Machine Intelligence*, vol. 25, no. 5, pp. 616-622, May 2003.
[4] X. Jiang and W. Ser, "Online Fingerprint Template Improvement," *IEEE Trans. Pattern Analysis and Machine Intelligence*, vol. 24, no. 8, pp. 1121-1126, Aug. 2002.
[5] S. Pankanti, S. Prabhakar, and A.K. Jain, "On the Individuality of Fingerprints," *IEEE Trans. Pattern Analysis and Machine Intelligence*, vol. 24, no. 8, pp. 1010-1025, Aug. 2002.
[6] Z.M. Kovacs-Vajna, "A Fingerprint Verification System Based on Triangular Matching and Dynamic Time Warping," *IEEE Trans. Pattern Analysis and Machine Intelligence*, vol. 22, no. 11, pp. 1266-1276, Nov. 2000.
[7] A.K. Jain, L. Hong, and R. Bolle, "On-Line Fingerprint Verification," *IEEE Trans. Pattern Analysis and Machine Intelligence*, vol. 19, no. 4, pp. 302-314, Apr. 1997.
[8] A.K. Jain, L. Hong, S. Pankanti, and R. Bolle, "An Identity-Authentication System Using Fingerprints," *Proc. IEEE*, vol. 85, no. 9, pp. 1365-1388, Sept. 1997.
[9] F. Galton, *Finger Prints*. Macmillan, 1892.
[10] A. Senior, "A Combination Fingerprint Classifier," *IEEE Trans. Pattern Analysis and Machine Intelligence*, vol. 23, no. 10, pp. 1165-1174, Oct. 2001.
[11] R. Cappelli, A. Lumini, D. Maio, and D. Maltoni, "Fingerprint Classification by Directional Image Partitioning," *IEEE Trans. Pattern Analysis and Machine Intelligence*, vol. 21, no. 5, pp. 402-421, May 1999.
[12] A.K. Jain, S. Prabhakar, and L. Hong, "A Multichannel Approach to Fingerprint Classification," *IEEE Trans. Pattern Analysis and Machine Intelligence*, vol. 21, no. 4, pp. 348-359, Apr. 1999.
[13] N.K. Ratha, K. Karu, C. Shaoyun, and A.K. Jain, "A Real-Time Matching System for Large Fingerprint Databases," *IEEE Trans. Pattern Analysis and Machine Intelligence*, vol. 18, no. 28, pp. 799-813, Aug. 1996.
[14] C.A.B. Smith, "Notes on the Forms of Dermatoglyphic Patterns," *Dermatoglyphics: Fifty Years Later*, Birth Defects: Original Article Series, vol. 15, no. 6, pp. 43-52, The Nat'l Foundation, 1979.
[15] K.V. Mardia, Q. Li, and T.J. Hainsworth, "On the Penrose Hypothesis on Fingerprint Patterns," *IMA J. Math. Applied in Medicine and Biology*, vol. 9, pp. 289-294, 1992.
[16] B.G. Sherlock and D.M. Monro, "A Model for Interpreting Fingerprint Topology," *Pattern Recognition*, vol. 26, no. 7, pp. 1047-1055, 1993.
[17] P.R. Vizcaya and L.A. Gerhardt, "A Nonlinear Orientation Model for Global Description of Fingerprints," *Pattern Recognition*, vol. 29, no. 7, pp. 1221-1231, 1996.
[18] J. Gu, J. Zhou, and D. Zhang, "A Combination Model for Orientation Field of Fingerprints," *Pattern Recognition*, vol. 37, pp. 543-553, 2004.
[19] L.S. Penrose, "Dermatoglyphics," *Scientific Am.*, vol. 221, no. 6, pp. 73-84, 1969.
[20] A.M. Bazen and S.H. Gerez, "An Intrinsic Coordinate System for Fingerprint Matching," *Proc. Third Int'l Conf. Audio- and Video-Based Biometric Person Authentication (AVBPA '01)*, pp. 198-204, 2001.
[21] C.I. Watson and C.L. Wilson, *NIST Special Database 4: Fingerprint Database*. Nat'l Inst. Standards and Technology, Mar. 1992.
[22] K. Bonnevie, "Studies on Papillary Patterns of Human Fingers," *J. Genetics*, vol. 15, no. 1, pp. 1-111, Nov. 1924.
[23] L.S. Penrose and P.T. Ohara, "The Development of Epidermal Ridges," *J. Medical Genetics*, vol. 10, no. 3, pp. 201-208, Sept. 1973.

[24] M. Kücken and A.C. Newell, "Fingerprint Formation," *J. Theoretical Biology*, vol. 235, no. 1, pp. 71-83, 2005.
[25] H. Grötzsch, "Über die Geometrie der schlichten konformen Abbildung," *Sitzungsberichte der Preussischen Akademie der Wissenschaften zu Berlin, Physikalisch-Mathematische Klasse*, pp. 654-671, 1933.
[26] O. Teichmüller, *Extremale quasikonforme Abbildungen und quadratische differentiale*, Abhandlungen der Preußischen Akademie der Wissenschaften, Mathematisch-naturwissenschaftliche Klasse, vol. 22, no. 1939. Verlag der Akademie der Wissenschaften, 1940.
[27] A.L. Kholodenko, "Use of Quadratic Differentials for Description of Defects and Textures in Liquid Crystals and $2+1$ Gravity," *J. Geometry and Physics*, vol. 33, nos. 1-2, pp. 59-102, 2000.
[28] S. Kerckhoff, H. Masur, and J. Smillie, "Ergodicity of Billiard Flows and Quadratic Differentials," *Annals of Math.*, second series, vol. 124, no. 2, pp. 293-311, Sept. 1986.
[29] M. Kontsevich and A. Zorich, "Connected Components of the Moduli Spaces of Abelian Differentials with Prescribed Singularities," *Inventiones mathematicae*, vol. 153, pp. 631-678, 2003.
[30] G. Jensen, "Quadratic Differentials," *Univalent Functions*, chapter 8, C. Pommerenke, ed. Vandenhoeck & Ruprecht, 1975.
[31] K. Strebel, *Quadratic Differentials*. Springer, 1984.
[32] C.L. Wilson, G.T. Candela, and C.I. Watson, "Neural Network Fingerprint Classification," *J. Artificial Neural Networks*, vol. 1, no. 2, pp. 203-228, 1994.
[33] J. Zhou and J. Gu, "Modeling Orientation Fields of Fingerprints with Rational Complex Functions," *Pattern Recognition*, vol. 37, pp. 389-391, 2004.
[34] D. Maio, D. Maltoni, R. Cappelli, J.L. Wayman, and A.K. Jain, "FVC2000: Fingerprint Verification Competition," *IEEE Trans. Pattern Analysis Machine Intelligence*, vol. 24, no. 3, pp. 402-412, 2002.
[35] A.M. Bazen and S.H. Gerez, "Systematic Methods for the Computation of the Directional Fields and Singular Points of Fingerprints," *IEEE Trans. Pattern Analysis Machine Intelligence*, vol. 24, no. 7, pp. 905-919, July 2002.
[36] J.A. Nelder and R. Mead, "A Simplex Algorithm for Function Minimization," *Computer J.*, vol. 7, pp. 308-313, 1965.

Stephan Huckemann received the PhD degree in mathematics from the University of Giessen, Germany, in 1987. He was a visiting lecturer and scholar at the University of Michigan, Ann Arbor, from 1987 to 1989 and a postdoctoral research fellow at ETH Zürich, Switzerland, from 1989 to 1990. He then worked as a commercial software developer and was a contributor to the computer algebra system MuPAD at the University of Paderborn, Germany, from 2001 to 2003. Currently, he holds a DFG research position at the Institute for Mathematical Stochastics, University of Göttingen, Germany. His research interests include pattern recognition, statistical shape analysis, and fingerprint modeling.

Thomas Hotz received a degree in mathematics from the University of Heidelberg, Germany, in 2002, and the PhD degree from the University of Göttingen, Germany, in 2007. He then worked as a research associate at the Department of Epidemiology and Public Health, University of Leicester, UK. Afterward, he held the position of associate statistician at the United Nations Statistics Division, New York, before returning to Germany. He currently works as a postdoctoral research fellow in the Institute for Mathematical Stochastics, University of Göttingen. His research interests include mathematical and statistical methods in image analysis, particularly in the analysis of fingerprints.

Axel Munk received a degree in mathematics and the PhD degree from the University of Göttingen, Germany in 1992 and 1994, respectively. He is the director of the Institute for Mathematical Stochastics, University of Göttingen. His current research interests include nonparametric statistics, medical statistics, and statistical inverse problems. He is guest editor of *Statistica Neerlandica*, the *Drug Information Journal*, and the *Biometrical Journal*. In 1992, he received the Gustav Adolf Lienert Award of the International Biometric Society, German Section. From 1992 to 1994, he was supported by the "Studienstiftung des Deutschen Volkes" and, afterward, by the German Research Foundation (DFG) until 1995. He was recently awarded a research semester on "Inverse Statistical Problems under Qualitative Prior Information" by DFG.